Study of the reversible/irreversible character of the deactivation of CuO/SBA–15 SOx adsorbents in wet conditions under SO2 adsorption/regeneration cycling experiments

Grégory Guicheney, Sophie Dorge, Habiba Nouali, Bénédicte Lebeau, M. Soulard, J. Patarin, M. Molière, M. Vierling, A.C. Houdon, Loic Vidal, et al.

Study of the reversible/irreversible character of the deactivation of CuO/SBA-15 SOx adsorbents in wet conditions under SO_2 adsorption/regeneration cycling experiments

G. Guicheney[a,b,c,d], S. Dorge[a,c*], H. Nouali[b,c*], B. Lebeau[b,c], M. Soulard[e], J. Patarin[e], M. Molière[e,f], M. Vierling[g], A.C. Houdon[d], L. Vidal[b,c], J.F. Brilhac[a,c]

[a] Université de Haute-Alsace, LGRE UR 2334, 3 bis rue Alfred Werner, 68100 Mulhouse, France
[b] Université de Haute-Alsace, CNRS, IS2M UMR 7361, 3 bis rue Alfred Werner, 68100 Mulhouse, France
[c] Université de Strasbourg, 67000 Strasbourg, France
[d] ADEME, 20 avenue du Grésillé, BP 90406, 49004 Angers Cedex 01, France
[e] Zéphir Alsace SAS, 68450 Brunstatt-Didenheim, France
[f] Université de Technologie de Belfort-Montbéliard (UTBM), ICB-LERMPS, Belfort, France
[g] GE Energy, 20 avenue du Maréchal Juin, 90007, Belfort Cedex, France

*Corresponding authors: sophie.dorge@uha.fr, habiba.nouali@uha.fr

Abstract

The effect of water vapor on the DeSOx performance of regenerable CuO/SBA-15 adsorbent was investigated for different temperatures of adsorption/regeneration cycles and CuO loadings. At 400 °C a significant decrease of both dynamic and total SO_2 adsorption capacity compared to the ones measured without water was observed. This decrease could be related to a faster migration and aggregation of the CuO active phase, an adsorption competition between water and SO_2 molecules on the active sites and/or the formation of copper based sulfate/oxysulfate/hydroxy-oxysulfate species difficult to decompose during the reductive regeneration step. On the other hand, at 450 °C water vapor leads to an increase of the total SO_2 adsorption capacity by more than 20%, which might be due to an acceleration of the oxidation of SO_2, a faster chemisorption of the sulfur species on the active sites and a more efficient regeneration step with regard to 400°C. The decrease of the CuO loading from 15 to 7 wt.% leads to a lower deactivation (i.e loss of SO_2 adsorption capacity) at the breakthrough of the adsorbent under wet conditions. Whatever the temperature and the CuO loading, once the water vapor is removed from the gas stream, the dynamic SO_2 adsorption capacities are totally or partially recovered. This behavior shows that the deactivation of the CuO/SBA-15 adsorbent induced by water vapor is a reversible or partially reversible phenomenon. It appears that during the DeSOx process a migration towards the pore mouth and an aggregation of the CuO active phase occur faster under water vapor conditions with the formation of large particles of CuO.

Keywords

DeSOx, CuO/SBA-15 adsorbents, adsorption/regeneration cycles, H_2O impact, reversible/irreversible deactivation

1. Introduction

Nowadays, sulfur oxides (SO_x with x = 2 or 3) are among the most closely monitored and regulated atmospheric pollutants in the world. Indeed, they induce harmful effects on the environment (acidification of lakes, forest dieback and degradation of architectural monuments, caused by acid rains

formed by reaction of SO_2 with the humidity of air [1]) and on the human health (respiratory [2] and cardiovascular [3] diseases, due to formation of sulfate aerosols and secondary organic aerosols [4]). The largest SO_2 emissions into the atmosphere are anthropogenic and mainly come from the flue gases generated by the combustion of sulfur-containing fossil fuels used by power plants but also in locomotives, ships, and other heavy-duty vehicles and equipment items. In order to meet the national and international regulations relating to the emissions of gaseous pollutants [5,6], Flue-Gas Desulfurization (FGD) processes have been largely installed by the power industries to reduce their SO_x emissions. However, the most commonly ones, which involve dry or wet scrubbing with alkaline materials, have the disadvantages of being costly and energy consuming, and moreover, they produce large amounts of waste that cannot be easily remarketed or disposed [7]. An alternative is the use of a dry and regenerable SO_x adsorbent like copper oxide supported on an ordered mesoporous SBA-15 silica, the CuO/SBA-15 adsorbent [8–16]. Indeed, this material boasts very attractive SO_x removal properties and interesting regenerative character, according the following adsorption and regeneration reactions (1), (2), (3a) and (3b):

Adsorption reactions:

$$SO_2 + ½\ O_2 \rightarrow SO_3 \text{ (oxidation of } SO_2) \quad (1)$$

$$SO_3 + CuO \rightarrow CuSO_4 \text{ (chemisorption of } SO_3) \quad (2)$$

Regenerative reactions:

$$CuSO_4 + 2H_2 \rightarrow SO_2 + Cu + 2H_2O \text{ (reductive regeneration)} \quad (3a)$$

$$2CuSO_4 + 3H_2 \rightarrow 2SO_2 + Cu_2O + 3H_2O \text{ (reductive regeneration)} \quad (3b)$$

Previous studies reveal that the total SO_2 adsorption capacity of this CuO/SBA-15 adsorbent can reach 100 $mg_{SO_2}/g_{adsorbent}$ and remains quite stable along a large number of adsorption/regeneration cycles in absence of water [14]. Moreover, the high thermal stability of the SBA-15 support and its chemical inertia with respect to SO_2 [17,18] allow the use of this adsorbent under the thermal conditions of the exhaust flue gas (i.e. 300-500 °C). Another advantage of this copper-based adsorbent is that during its regeneration, the trapped SO_x pollutants can be released and remarketed for the manufacturing of valuable products (e.g. for the production of sulfuric acid [19,20] or elemental sulfur [21]). Currently, the majority of the studies conducted to evaluate the potential of the CuO/SBA-15 adsorbent as an option for FGD [8–16] have been carried out under dry condition, i.e. without water vapor. However, the combustion of solid and liquid fossil fuels generates water vapor in the flue gas, which is likely to impact the activity of the SO_x adsorbents. For this reason, we have investigated in an previous work [22] the effects of water vapor on the performance of the CuO/SBA-15 as a SO_x adsorbent over multiple adsorption/regeneration cycles, looking more specifically at the influence of the process temperature and the CuO loading. It has been shown that when water vapor is present in the gas phase during the adsorption step, it can entail two distinct and apparently contradictory effects:

- When the process temperature range is from 350 to 400°C, water vapor causes (i) a loss by around 50 % of the "dynamic" SO_2 adsorption capacity (i.e. the capacity measured at the breakthrough), along the cycles, regardless of the operational conditions and (ii) a decrease of the total SO_2 storage capacity. These negative effects can be linked to (i) a faster migration and agglomeration of the CuO active phase in the presence of water vapor, (ii) an adsorption competition between water vapor and SO_2 on the active sites and/or (iii) the formation of copper based sulfate/oxysulfate/hydroxy-oxysulfate species, which are difficult to decompose during the reductive regeneration step.
- When the process temperature is 450 °C, water vapor causes an increase of the total SO_2 adsorption capacity by more than 15 % which can be explained by (i) an acceleration of the oxidation of SO_2, leading to a faster chemisorption of the sulfur species on the active sites and probably (ii) a more efficient regeneration step at this higher temperature.

The literature indicates that, when some water vapor is present in a gas phase being in reaction with a solid material, it generally impacts its performance [23–27], whatever the process used. However, in many cases, the activity is totally or partially recovered once H_2O is removed [28–34]. Indeed, various

authors, who have investigated on $DeNO_x$ processes involving supported metal oxides as catalysts, have reported both reversible and irreversible losses of the $DeNO_x$ activities. Iwamoto *et al.* [28] found that a Cu-MFI $DeNO_x$ catalyst using hydrocarbons as reducer, lost 35 % of its activity in presence of 3.9 % of H_2O at 500 °C, a phenomenon that was proved totally reversible after removing water vapor from the reacting gas. Kijlstra *et al.* [29] observed that the original $DeNO_x$ activity of a MnO_x/Al_2O_3 catalyst using ammonia as reducer was decreased by 70% in presence of 2 vol.% of H_2O at 150 °C; this loss was partially reversible, with a return to 85 % of the original activity when the injection of water vapor was suppressed. They assumed that the unrecovered fraction of the activity (corresponding to the "deactivation" effect) was due to a dissociative adsorption of water as superficial hydroxyls, while the recoverable fraction (corresponding to the "inhibition" effect) was caused by an adsorption competition between H_2O and the reactants (NO and NH_3). In addition, they showed that increasing the process temperature up to 425 °C, made both the inhibition and the deactivation effects of H_2O negligible. Liu *et al.* [30] also observed a loss of activity by 6 % of a Cu-Mn/SAPO-34 $DeNO_x$ catalyst in presence of 10 vol.% of H_2O at 240 °C, with an irreversible fraction of 2 %. They also explained the deactivation effect of water vapor by the formation of hydroxyls on the surface of the catalyst, created by the adsorption and decomposition of water molecules, a process which declines when the process temperature increases. Gholami *et al.* [31] reviewed the effect of H_2O on the activity of Pd catalysts used for the oxidation of unburned CH_4 at the exhaust of gas fired vehicles: they reported that, when Pd was supported on Al_2O_3 or zeolites (H-Beta, H-TNU-10), the catalysts suffered an inhibition effect of 5 to 86 % in presence of 5-10 vol.% of H_2O at 400-600 °C, the definitive deactivation figure varying between 2 and 68 %. They also reported that several authors assigned the deactivation to a reaction between H_2O and the PdO active phase, resulting in the formation of inactive $Pd(OH)_2$ sites. This reaction could be reversed at higher temperatures (above 450 °C), probably due to the decomposition of that hydroxide. Furthermore, they consider the migration and coalescence of the active Pd atoms as another cause of the deactivation. As shown by Lamber *et al.* [35] with a Pd/SiO_2 catalyst, the presence of H_2O induces the formation of silanol (Si-OH) groups favoring the migration and the coalescence of the Pd atoms. Importantly, the oxidation state of the active metallic sites can affect the migration effect over the support, as pointed by Xu *et al.* [36]. Indeed, they observed that the total decomposition of the PdO active phase to the metallic one (Pd^0) resulted in a faster agglomeration of the palladium species on the Al_2O_3 support.

Reversible deactivations of catalysts are also observable in the SCR technology as shown by the study of Tong *et al.* [37] who investigated the effect of 10 vol.% of H_2O on the activity of a $CuSO_4$-CeO_2/TiO_2-SiO_2 catalysts at different temperatures. They observed that when water vapor was introduced into the feed gas for four hours, the conversion of NO decreased down to 3 %, 6 % and 23 % of the initial value, at 220 °C, 200 °C and 180 °C respectively. After cutting off H_2O, the NO_x removal activity was restored quickly to its original level regardless of the temperature. They proposed a competitive adsorption of H_2O molecules on the catalyst to explain this phenomenon.

In view of this background and the desulfurization process under consideration, the purpose of this work is to study the evolution of the $DeSO_x$ performance of the CuO/SBA-15 adsorbent along adsorption/regeneration cycles in presence of water vapor. To that end, the chosen strategy has been to alternate adsorption phases with and without water vapor in the gaseous stream and to investigate the resulting effects both in terms of adsorbent efficiency and adsorbent structural properties. The primary goal is to determine whether the deactivation is reversible or irreversible and identify the role played by H_2O in these losses of activity. Then, a key point is to be able to modify the adsorbent and/or the operating conditions of the process, to eliminate or limit this negative impact of H_2O. This improvement is actually necessary to envisage a potential industrial application of this regenerative $DeSO_x$ process as a replacement for the current FGD technologies.

2. Materials and methods

2.1. Elaboration of the CuO/SBA-15 adsorbents

2.1.1. Synthesis of the SBA-15 support

The SBA-15 silica support was synthesized in a large amount, according the procedure used in a previous work [22]: 196 g of porogen agent (Pluronic® P123, Sigma-Aldrich) was dissolved in 1,121 g of HCl (37 wt.%, Carlo Erba) and 6,387 g of demineralized water, at 45 °C for 12 h. Then, 425 g of silica precursor (Tetraethylorthosilicate, Evonik) was added to the solution, which was kept under stirring for 4 h at 45 °C. Afterward, the mixture was heated up to 90 °C for 18 h, under static mode and autogenous pressure. The white precipitate obtained was recovered by centrifugation, washed with demineralized water until the washing water was at the pH of demineralized water and dried overnight at 60 °C for 24 h in a ventilated oven. In order to eliminate the porogen agent trapped in its mesopores, the as made SBA-15 material was then calcined at 300 °C under air flow in a muffle furnace with a temperature ramp of 1 °C.min^{-1} up to 300 °C and a plateau of 4 h at 300 °C. An amount of about 120 g of calcined SBA-15 was obtained.

2.1.2. Deposition of the CuO active phase on the support

Two adsorbents with different CuO active phase contents were studied: with 7 and 15 wt.%. The deposition of the copper species on the SBA-15 support was realized by wet impregnation, using $Cu(NO_3)_2.3H_2O$ as precursor (employed as received without further purification). Desired amount of precursor (0,686 and 1,608 g for a 7 and 15 wt.% loading, respectively) was dissolved in 20 mL of demineralized water. Then, 3 g of calcined SBA-15 material was introduced and mixed at room temperature for 4 h. Next, the most part of the solvent was completely evaporated by heating the mixture with a water bath at 60 °C under stirring. Then, the resulting powder was completely dried at 60 °C for 24 h in a ventilated oven and then calcined according to the following conditions: in a fixed-bed reactor, with 10 mm adsorbent bed thickness, under an air flow, with a Gas Hourly Space Velocity of 15,000 h^{-1}, with a temperature ramp of 1 °C.min^{-1} up to 500 °C followed by 6 h stage at 500 °C and a cooling of 1 °C.min^{-1} up to room temperature. The obtained adsorbents are designated afterwards as "XCuO/SBA-15", where X corresponds to the CuO wt.% loading determined by X-Ray Fluorescence.

2.2. Evaluation of the cyclic SO_2 adsorption and regeneration performance of the adsorbents: $DeSO_x$ test

The SO_2 adsorption and regeneration properties of the CuO/SBA-15 adsorbents were evaluated under cyclic adsorption/regeneration tests ($DeSO_x$ tests) globally performed on a 20 mm thick adsorbent bed previously shaped in 32 mm diameter tablets (0.25 t/cm² for 2 min), manually crushed (with mortar and pestle) and sieved within the 250-355 µm range. Deposited on a frit in a U-shaped reactor, the adsorbent was firstly heated up to the desired temperature (400 or 450 °C) under pure N_2 flow, with a heating rate of 5 °C.min^{-1} and followed by 1 h stage. Next, the adsorption step was launched during 3,000 s or 10,800 s with an inlet gas stream composed of 250 ppm of SO_2 and 10 vol.% of O_2 diluted in N_2. For the tests performed under wet conditions, 5 vol.% of H_2O was added in the inlet gas stream, through an evaporator system. Afterward, the regeneration step was carried out at the same temperature that the one of the adsorption step (isothermal process), under a reductive atmosphere composed of 0.5 vol.% of H_2 diluted in N_2, during 1,500 s. Between adsorption and regeneration steps, a pure N_2 flow was imposed for 600 s. At the outlet of the reactor, the concentration of SO_2 in the gas phase was determined online with an UV SO_2 adsorption analyzer (Rosemount X'Stream). All along the test, the gas was maintained at a Gas Hourly Space Velocity of 25,000 h^{-1} (i.e. with a volumetric flow rate of 14 NL.h^{-1}).

In this study, the SO_2 adsorption and regeneration performance of the different CuO/SBA-15 adsorbents was evaluated along cycling experiments according to the evolution of two different data: the SO_2 adsorption capacity at the breakthrough $C_{SO_2}^{breakthrough}$ and the total SO_2 adsorption capacity $C_{SO_2}^{total}$. These capacities, expressed in mg of adsorbed SO_2 per gram of active phase (CuO), were determined from the integration of the SO_2 breakthrough curves (established during the adsorption step) until the SO_2 concentration at the reactor outlet reaches 5 ppm and from the integration of the SO_2

desorption curves (established during the regeneration step), according to equations (4) and (5) respectively:

$$C_{SO_2}^{breakthrough} = \frac{F_v \times \int_{t_1}^{t_b} (C_0 - C) dt}{10^3 \times V_m \times m_{CuO}} \times M_{SO_2} \quad (4)$$

$$C_{SO_2}^{total} = \frac{F_v \times \int_{t_2}^{t_f} C \, dt}{10^3 \times V_m \times m_{CuO}} \times M_{SO_2} \quad (5)$$

Where F_v (in NL.h^{-1}) is the gas volumetric flow rate. C_0 and C (in ppm) are the reactor inlet and outlet SO_2 concentrations respectively. t_1 and t_2 (in h) are the starting times of the adsorption step and the regeneration step, respectively. t_b and t_f (in h) are the time at the SO_2 breakthrough (when 5 ppm of SO_2 is detected from the analyzer) and the final time of the regeneration step, respectively. V_m is the molar volume of a gas (22.4 L.mol^{-1} at 0 °C and 1 atm). m_{CuO} is the mass of active phase CuO in the adsorbent within the fixed-bed (in g). M_{SO_2} is the molar mass of SO_2 (64 g.mol^{-1}).

The sulfation ratio of the CuO active phase was also calculated (in %) from the ratio between the molar quantity of SO_2 adsorbed (in $mol_{SO_2}/g_{adsorbent}$) to the molar quantity of CuO content in the adsorbent (in $mol_{CuO}/g_{adsorbent}$).

2.3. Characterization techniques

2.3.1. X-Ray Fluorescence (XRF)

The CuO active phase loading of the adsorbent was determined with a X-Ray Fluorescence spectrometer Zetium from Panalytical and based on a homemade bulk CuO standard compound. The analysis was carried out on a sample compacted in a 13 mm diameter pellet.

2.3.2. X-Ray powder Diffraction (XRD)

The structural properties of the adsorbents were evaluated by X-Ray powder Diffraction (XRD). The analyses were realized in reflection mode on a X'Pert PRO MPD Powder diffractometer from Panalytical, equipped with a X'Celerator detector and a sample changer. Measurements were achieved with $Cu_{K\alpha}$ radiation ($\lambda_{K\alpha}$ = 0.15418 nm), for 2θ angle values range from 0.02 to 70 ° (0.02 °/step, 220 s/step) and a fristed glass plate as sample holder.

2.3.3. Nitrogen adsorption/desorption measurements

The textural properties of the adsorbents were assessed by measurements of adsorption and desorption isotherms (at -196 °C) of nitrogen, carried out on a Micromeritics Tristar sorptometer. Before measurements, samples were outgassed at 150 °C for 15 h under vacuum (10^{-3} mbar). The microporous and total pore volumes were measured at relative pressures P/P_0 = 0.005 (according to the work of Galarneau et *al.* [38]) and P/P_0 = 0.9, respectively. The mesoporous volume was calculated by microporous and total porous volumes difference. The specific surface area was determined by the BET (Brunauer-Emmett-Teller) method (in the range P/P_0 = 0.05-0.35) [39]. The average mesopore size is evaluated by the maximum of the pore size distribution obtained by the BJH (Barrett-Joyner-Halenda) method applied to the desorption branch [40].

2.3.4. Transmission Electron Microscopy (TEM) and Energy Dispersive X-ray (EDX) mapping

Transmission Electron Microscopy (TEM) and Energy Dispersive X-ray (EDX) mapping images were obtained on an Jeol ARM-200F microscope equipped with a LaB_6 filament and an EDX Jeol Centurio detector. First, samples were dispersed in chloroform and sonicated during 10 min. Next, two to three drops of the solution were deposited onto gold grids coated with a 5 nm thickness of holey carbon film. These characterization techniques were used particularly to evaluate the dispersion state of the CuO active phase on the SBA-15 support. From EDX mapping analyses, the variation of the copper oxide dispersion (in %) was calculated according to equation (6). This parameter was defined to estimate qualitatively the CuO dispersion state change in the adsorbents after $DeSO_x$ test. For this purpose, with the help of copper EDX maps, "surface" CuO load corresponding to atomic % of Cu was measured on homogeneous areas, free of nanoparticles, before and after $DeSO_x$ test (see selected areas in **Figure 6**) and compared to each other. Thus, a variation of the CuO dispersion of 50 % indicates that the initial CuO dispersion state has decreased by half.

$$CuO\ dispersion\ variation = \left(1 - \frac{"Surface\ CuO\ load"\ of\ the\ spent\ adsorbent}{"Surface\ CuO\ load"\ of\ the\ fresh\ adsorbent}\right) \times 100 \qquad (6)$$

2.3.5. Inductive Coupled Plasma Optical Emission Spectroscopy (ICP-OES)

The quantification of sulfur in the adsorbents was performed by ICP-OES analyses. Before analysis, the samples underwent two acid digestions: the first one occurs at room temperature for 24 hours (0.035 to 0.075 g of sample are added to 1 mL of 48.9% hydrofluoric acid (HF)). The second one is performed with the addition of 4 mL of 69% nitric acid (HNO_3). Then, the obtained solution was diluted to 50 mL with demineralized water and filtered through a 0.45 µm filter after the neutralization of HF by boric acid. The solution was then analyzed using an ICAP 6300 DUO instrument (Thermo, Villebon-sur-Yvette).

3. Results and discussion

In order to evaluate the impact of the presence of H_2O in the gas phase during the SO_2 adsorption step, on the SOx trapping performance along cycling experiments of our CuO/SBA-15 adsorbent, an extensive series of 50 adsorption/regeneration cycles was performed on this adsorbent while alternating wet gas steams (with 5 vol.% of H_2O during cycles 1 to 30 and 41 to 50) and dry ones (without H_2O during the cycles 31 to 40). The aim is to understand the mechanisms which occur and may cause irreversible or reversible damages on the material in presence of water vapor for the implementation of an efficient solution to prevent and/or limit the possible deactivation, particularly by adjusting the temperature of the process and the amount of copper active phase on the silica support SBA-15.

The influence of three parameters relating to the adsorption phases has been studied:

- Temperature: 400 and 450 °C, with a 15CuO/SBA-15 adsorbent undergoing 10,800 s of SO_2 adsorption phases
- Amount of the active phase: 7 and 15 wt.% of CuO, at 450 °C using a constant SO_2 adsorption time (10,800 s)
- Duration of the SO_2 adsorption phase: 3,000 and 10,800 s, using a constant CuO content (15 wt.%) in the adsorbent and a constant temperature (450 °C).

For this, the evolution of both the SO_2 adsorption capacity at the breakthrough and the total SO_2 adsorption capacity was monitoring throughout all this cycle sequence. These two capacities $C_{SO_2}^{breakthrough}$ and $C_{SO_2}^{total}$ represent two distinct properties of the adsorbent: the first one corresponds to its reactivity for the trapping of SO_2 while the second one to its intrinsic total SO_x storage capacity. They are also probably associated with the sulfation of different sites: $C_{SO_2}^{breakthrough}$ could correspond to the sulfation of the most accessible sites, i.e. the surface sites of the active phase particles and $C_{SO_2}^{total}$ represents the sulfation of all the sites in the adsorbent, including the less active surface ones and those located in the core of the active phase particles (CuO particles).

Based on this investigation plan, the results will be presented in successive sections, that will be treated independently and deal with the evolution of these two capacities along the cycles.

Moreover, an additional sequence of twenty cycles without the injection of water vapor during the adsorption phase was also performed on the adsorbent, to better assess the impact of the presence of H_2O on the performance of the CuO/SBA-15 adsorbent.

3.1. Evolution of the SO_x trapping and regeneration performance of CuO/SBA-15 adsorbents along 50 cycles alternating wet and dry conditions

The evolution of the SO_2 adsorption capacity at the breakthrough and the total SO_2 adsorption capacity, as well as the breakthrough and desorption curves of the different tests are reported in **Figures 1, 2 and 3,** respectively.

3.1.1. Evolution of the SO_2 adsorption capacity at the breakthrough

Influence of temperature

When comparing the capacities at the breakthrough $C_{SO_2}^{breakthrough}$ (**Figure 1.a**) measured during the first 20 adsorption-regeneration cycles with and without H_2O (full lines curves with and without motifs, respectively) in the gas phase during the adsorption step, a negative impact of water vapor on the SO_x trapping performance of the 15CuO/SBA-15 adsorbent, regardless of the temperature, was observed. Indeed, the $C_{SO_2}^{breakthrough}$ are lower in the presence of water vapor at both temperature 400 and 450 °C, with a progressive but important decrease along the first thirty cycles. This decrease leads to a capacity loss of 78 and 75 % of the initial $C_{SO_2}^{breakthrough}$, at cycle 30, at 400 and 450 °C, respectively (**Figure 1.a**). The decrease is faster at 400 °C and occurs during the first twenty cycles before a stabilization of the SO_2 adsorption capacity value. The capacity loss caused by water vapor at 450 °C, even reaches 85 % at cycle 50 and can be explained by an acceleration of the migration and agglomeration of the CuO active phase particles along the successive cycles with temperature, as shown below when dealing with the structural analyses of the spent materials. This effect of agglomeration of the CuO active phase particles at both temperatures causes a decrease of the number of the most active sites for the SO_2 adsorption reactions which are the surface sites. This modification is likely to explain the loss of reactivity of the adsorbent particularly for the oxidation of SO_2 in SO_3. This point is consistent with the modification of the shape of the SO_2 breakthrough curves (**Figures 2.a, d**) that become increasingly steep along the cycle sequence, particularly at 400 °C (**Figure 2.a**) and with the breakthrough time that decreases along the first 30 cycles.

For the first 30 cycles of adsorption-regeneration, the value of $C_{SO_2}^{breakthrough}$ is higher at 450 °C than at 400 °C in presence of water vapor (cycle 1: 350 versus 230 mg_{SO_2}/g_{CuO} and cycle 30: 80 versus 50 mg_{SO_2}/g_{CuO} at 450 and 400 °C, respectively). This point can be explained by different factors:

(1) The activation of the $DeSO_x$ process, since increasing temperature enhances the overall reactivity of the CuO active phase for the SO_x adsorption reactions (i.e. the oxidation of SO_2 and the chemisorption of SO_3). As reflected by the portion of the adsorption curves after the breakthrough, at the end of the adsorption step, it is interesting to note that less than the 250 ppm of the injected SO_2 is detected, whatever the temperature (400 and 450 °C). This indicates that the adsorbent is still able to oxidize SO_2 to SO_3 after 10,800 s of sulfation of the active phase. However, lower SO_2 emissions are observed at 450 °C (**Figure 2.d**) than at 400 °C (**Figure 2.a**), which accounts for a better oxidation of SO_2 in SO_3 (not detected by the analyzer) at 450 °C.

(2) A strong blocking of the active sites at lower temperature. Indeed, lower temperatures could favor the stability of hydroxyl copper species which are assumed to be formed by dissociative adsorption of water vapor on the most active sites [25].

(3) The formation of sulfated copper species which are difficult to decompose under the regenerative conditions applied (400 °C, 0,5 vol.% H_2 in N_2) during the regeneration step, such as basic copper sulfate hydroxides ($CuO.CuSO_4.2Cu(OH)$ which are stable up to 400 °C [41] or copper oxysulfates [42].

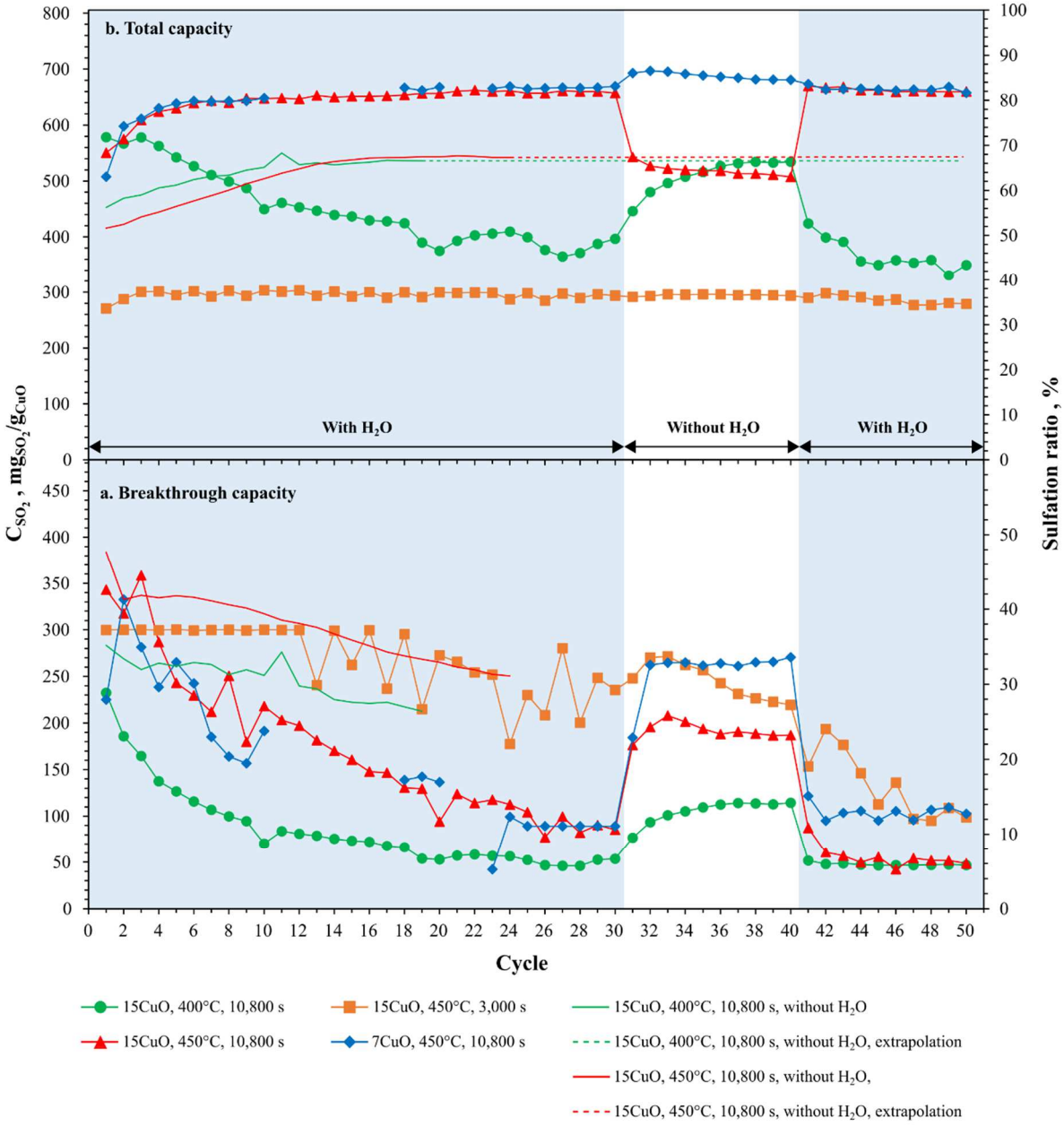

Figure 1: Evolution of the SO_2 adsorption capacities at the breakthrough (a) and the total SO_2 adsorption capacities of the CuO/SBA-15 adsorbents (b), submitted to 50 SO_2 adsorption/regeneration cycles with or without H_2O during the adsorption step.

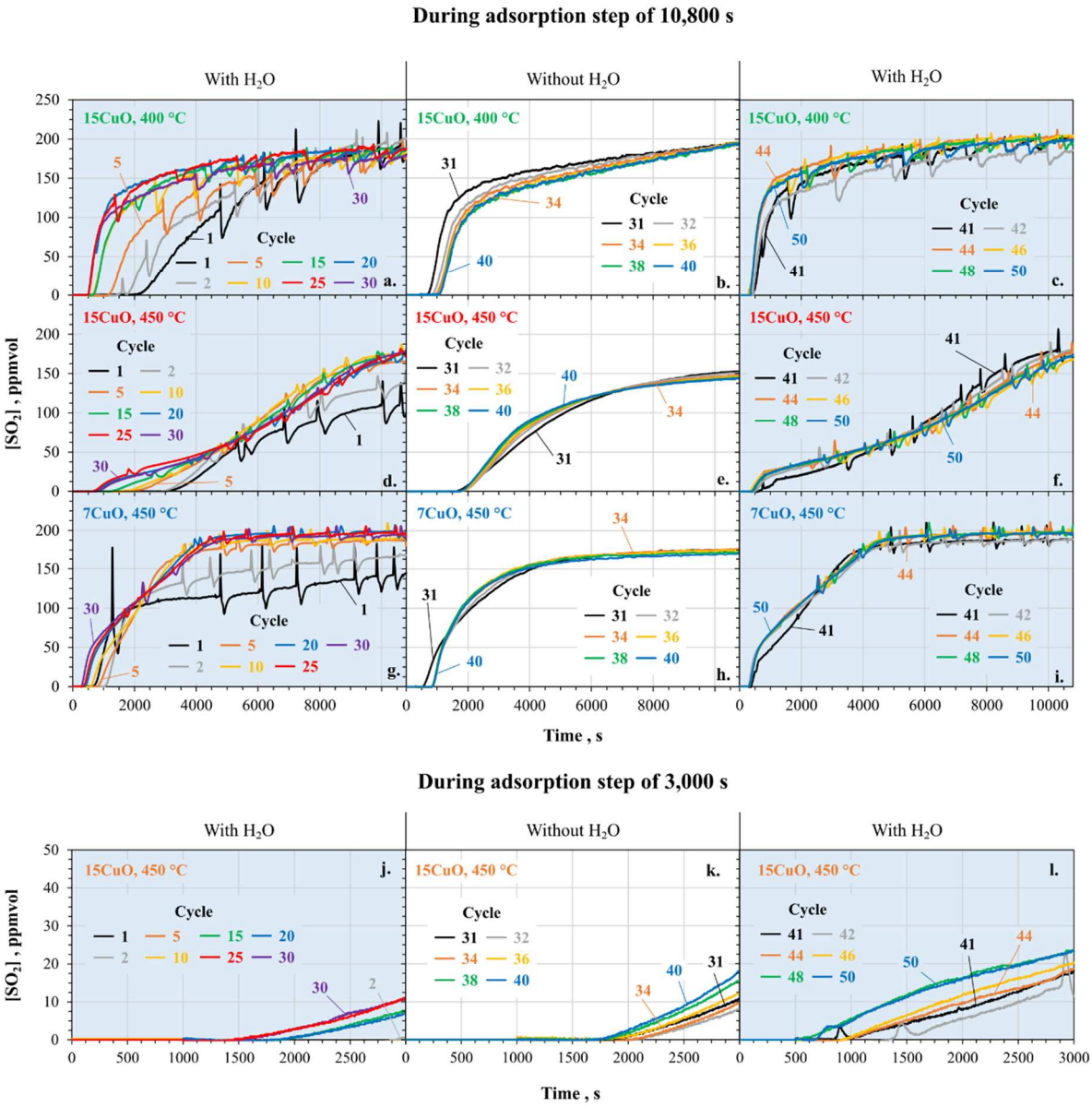

Figure 2: SO_2 breakthrough curves of the CuO/SBA-15 adsorbents, submitted to 50 SO_2 adsorption/regeneration cycles with or without H_2O during the adsorption step.

During the following cycles that are free of H_2O (cycles 31 to 40), the data $C_{SO_2}^{breakthrough}$ increases again up to 48 and 54 % of the initial capacity, at 400 and 450 °C, respectively (**Figure 1.a**). It is traduced on the adsorption curves, by an increase of the breakthrough time (**Figures 2.b, e**). The increase of $C_{SO_2}^{breakthrough}$ highlights the fact that the deactivation of the 15CuO/SBA-15 adsorbent caused by H_2O is partially reversible. The increase of the performance is faster at 450 °C with the SO_2 adsorption capacity becoming stable at cycle 32, whereas at 400 °C the increase is very progressive. This finding indicates that the temperature strongly affects the reversibility of the deactivation, which is improved when the temperature increased. At 450 °C, the stopping of the water vapor injection permits to immediately retrieve the major part of the initial performance of the adsorbent (around 55 %) and to slightly reduce the SO_2 emissions at the end of the adsorption step. This means that at this temperature, the deactivation in presence of H_2O, is probably due to a blocking of the active sites of the 15CuO/SBA-15 adsorbent by water vapor, the phenomenon of blocking being non-permanent. Nevertheless, this deactivation is partially irreversible since one does not fully recover the initial performance, probably

due to an agglomeration of the CuO active phase which is an irreversible evolution of the material accelerated in presence of water vapor. At lower temperature (400 °C), the fact that the increase of the SO_2 adsorption capacity is progressive from cycle 31, probably reflects the fact that the blocking process of some active sites caused by H_2O is coupled with the formation of sulfated copper species that are difficult to regenerate at this temperature in presence of H_2 (0.5 vol.% in N_2). This viewpoint will be further discussed when studying the desorption curves developed during the regeneration step.

When water vapor is reintroduced into the gas mixture over the last adsorption/regeneration cycles (cycles 41 to 50), the data $C_{SO_2}^{breakthrough}$ quickly decreases to the same level as before the removal of water vapor and this is observed at both temperatures (**Figure 1.a**). This finding supports the assumption that the reversible part of the deactivation is linked to a non-permanent blocking of the active sites by water vapor and that the non reversible part is most likely caused by an agglomeration effect of the active phase accelerated by H_2O, which is an irreversible phenomenon.

Influence of the CuO active phase loading

The decrease of the active phase content from 15 to 7 wt.% of CuO in the adsorbent, shows that along the first 30 cycles performed with water vapor at 450 °C, the deactivation of the 7CuO/SBA-15 along the cycles is similar to the one observed with the 15CuO/SBA-15 (**Figure 1.a**). Indeed, whatever the CuO active phase loading in the adsorbent, the $C_{SO_2}^{breakthrough}$ progressively decreases down to the same level of SO_2 adsorption capacity (90 mg_{SO_2}/g_{CuO}). This deactivation is also noticed on the SO_2 breakthrough curves obtained during the 30 first cycles (**Figure 2.g**) which show a decrease of both the breakthrough time and the SO_2 outlet concentration value at the end of the adsorption step, along the cycle sequence. Nevertheless, when the injection of H_2O in the gas phase to be treated is stopped at cycle 31, the 7CuO/SBA-15 adsorbent rapidly recovers near 80 % of its initial $C_{SO_2}^{breakthrough}$ (during cycle 32, see **Figure 1.a**). For this adsorbent, the irreversible part of the deactivation is less important than the one of the 15CuO/SBA-15 (20 % versus 45 % of the initial $C_{SO_2}^{breakthrough}$). This interesting finding is probably linked to the lower copper oxide concentration, which induces a more stable dispersion of the CuO active phase particles on the support and thus a better retention of the reactivity of the copper species for the adsorption reactions, this point was discussed in our previous work [22] and is confirmed by the transmission electron microscopy analyses (*vide infra*). This stability of the CuO dispersion at the lower concentration of CuO (7 wt.%) induces a higher and more stable $C_{SO_2}^{breakthrough}$ at around 100 mg_{SO_2}/g_{CuO} (cycle 41 to 50) than the one obtained with a higher concentration of CuO (15 wt.%) for which $C_{SO_2}^{breakthrough}$ continues to decrease from around 90 to 50 mg_{SO_2}/g_{CuO} (cycle 41 to 50).

It is noteworthy that the SO_2 breakthrough curves for both the 7CuO/SBA-15 and 15CuO/SBA-15 adsorbents and whatever the temperature (400 or 450 °C) are similar from cycle 31 to 40 (**Figures 2.b, e, h**), indicating a stability of the adsorbents. Likewise, when H_2O was again injected (cycles 41 to 50) the shape of all breakthrough curves is similar to the one at cycle 30, indicating again a stability of the performance of the adsorbent (**Figures 2.c, f, i**).

Influence of the duration of the adsorption step

It should be noted that the duration of 3,000 s of adsorption was selected in order to correspond to the time for which no SO_2 emission is detected, considering the $DeSO_x$ tests performed in a previous work ([22] in SI) on a 16 wt.% CuO loading on SBA-15 adsorbent at 450 °C without H_2O.

The 15CuO/SBA-15 adsorbent deactivation in presence of water vapor, is reduced by the decrease of the adsorption step duration (3,000 s), at 450 °C. Indeed, from **Figure 1.a**, the decrease of the value $C_{SO_2}^{breakthrough}$ after 30 cycles, is lower with an adsorption phase of 3,000 s (around 27 % of decrease), compared to the one with an adsorption duration of 10,800 s (75 % of decrease). This decrease of

performance of the 15CuO/SBA-15 with an adsorption step of 3,000 s is also observable on the breakthrough curves (**Figure 2.j**), where the breakthrough time decreases along the cycle sequence in presence of water vapor. Indeed, no SO_2 emission is observed for cycle 1 to 5 during 3,000 s, whereas for cycle 15 to 30, the breakthrough occurs at 1,500-1,700 s. After stopping H_2O injection, the breakthrough time increases again from 1,500 (cycle 30) to 1,900 s (cycle 31) (**Figure 2.k**) and decreases after reinjection of H_2O from 1,700 (cycle 40) to 900 s (cycle 41) (**Figure 2.l**). However, looking at the shape of the breakthrough curves, it appears that the adsorbent seems stabilized only from cycle 48 to reach a high value of $C_{SO_2}^{breakthrough}$ (90 mg_{SO_2}/g_{CuO}, **Figure 1.a**) compared to the one reached with a 10,800 s of adsorption time (close to 50 mg_{SO_2}/g_{CuO}). It is obvious that the decrease of the adsorption duration allowed to slow down the deactivation of the adsorbent. Shorter cycle duration could be beneficial within industrial applications.

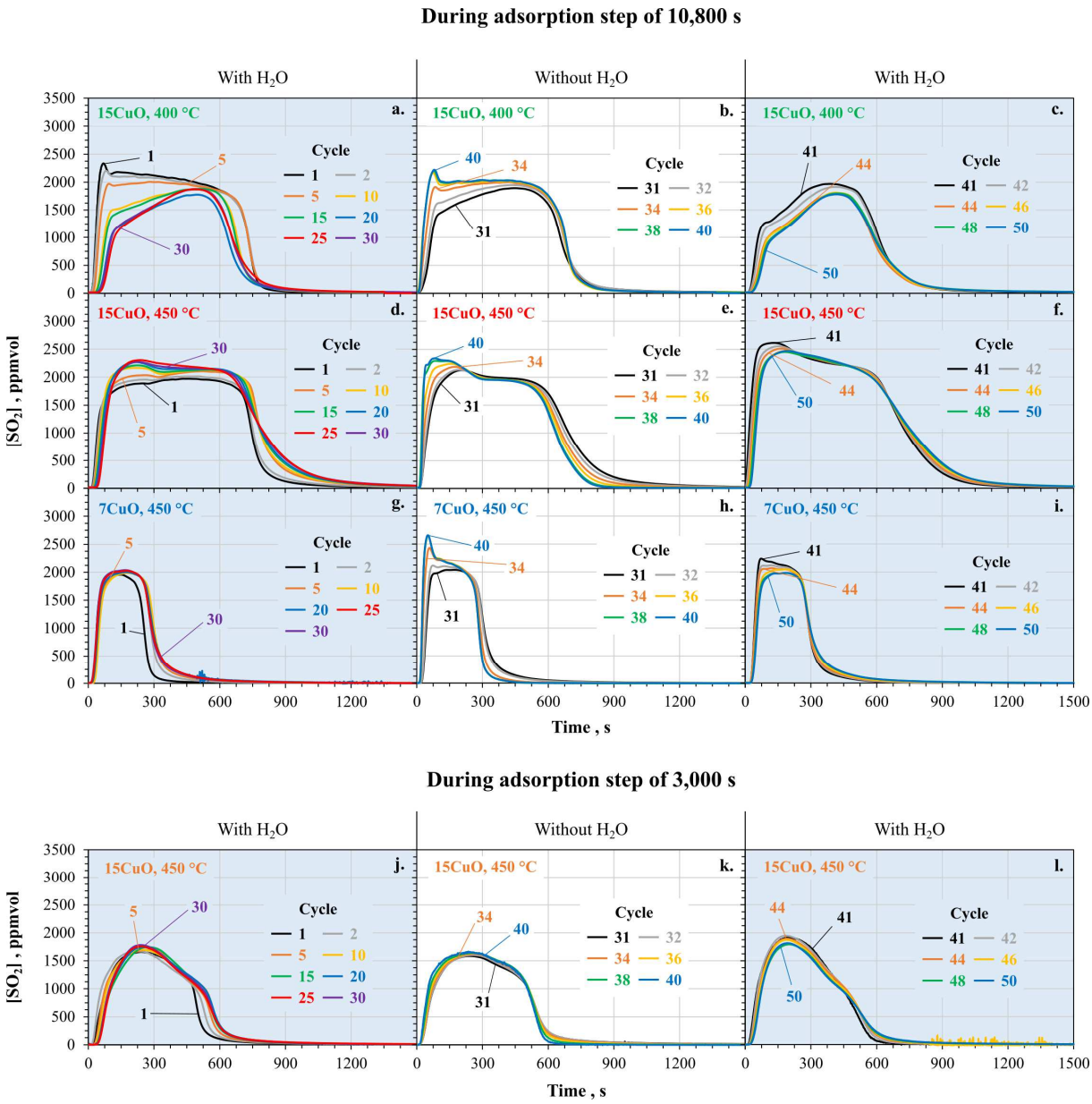

Figure 3: SO_2 desorption curves of the CuO/SBA-15 adsorbents, submitted to 50 SO_2 adsorption/regeneration cycles according series with or without H_2O during the adsorption step.

3.1.2. Evolution of the total SO_2 adsorption capacity

The total SO_2 adsorption capacity $C_{SO_2}^{total}$ corresponds to the total amount of SO_2 trapped by the adsorbent during the entire adsorption step and generated upon the regeneration step (**Figure 1.b**). The shape of the SO_2 desorption curves will depend on the nature and accessibility of the sulfated sites and of course of the regeneration conditions (**Figures 3.a-l**).

Temperature influence

At 450 °C, it clearly appears that the presence of H_2O vapor has a promoting effect on the total SO_2 adsorption capacity $C_{SO_2}^{total}$ of the 15CuO/SBA-15. At this temperature, the values of $C_{SO_2}^{total}$ measured in presence of H_2O are higher than the ones measured in dry conditions (full line red curve without motifs on **Figure 1.b**). Indeed, a gain of more than 20 % is obtained when injecting water vapor during the first thirty cycles, with a stable total SO_2 adsorption capacity of 660 mg_{SO_2}/g_{CuO} from cycle 12 to cycle 30 at 450 °C in presence of H_2O. Moreover, stopping of the injection of water vapor during cycles 31 to 40, clearly induces a decrease by 20 % of the total capacity at this temperature. When the water vapor is reintroduced in the gas phase from cycle 41 to 50, the total capacity increases again up to the value measured before the stopping of the injection of H_2O (cycle 30) and moreover, stays stable until the end of the cycling experiments. It is assumed that at this temperature, H_2O induces the formation of sulfite/sulfate species (SO_3^{2-}, SO_4^{2-}) on the most reactive sites (surface sites of the copper particles), which are more easily regenerable at this temperature, resulting in a more extensive sulfation reaction [28].

At 400 °C, the behavior of the 15CuO/SBA-15 adsorbent in presence of water vapor is different. The positive effect of H_2O on the total SO_2 adsorption capacity is only observed during the first five cycles. The $C_{SO_2}^{total}$ starts to decrease from cycle 4 in presence of H_2O, unlike experiments in dry conditions where it increases along the 15 first cycles and stay constant for the additional cycles (from cycle 19 to 30) (full lines green curve without motifs on **Figure 1.b**). The decrease of $C_{SO_2}^{total}$ in presence of H_2O reaches 28 % at cycle 19 with a value of $C_{SO_2}^{total}$ around to 380 mg_{SO_2}/g_{CuO} at 400 °C. This value of SO_2 adsorption capacity which corresponds to a sulfur content in the adsorbent of 2.7 wt.%, is validated by ICP-OES analysis of the sulfated material at 400 °C after the adsorption step of cycle 30 (2.6 wt.% by ICP-OES). The positive effect of the presence of H_2O, which is also expected to generate sulfite/sulfate species, is probably compensated by a deactivation process which becomes more and more pronounced along cycles at lower temperature of 400 °C. This deactivation, as noted above, could be explained by the formation of copper based sulfate/oxysulfates/hydroxy-oxysulfate species at the surface of the copper-based particles that are very difficult to decompose at the temperature of 400 °C. The amount of these compounds increases during the successive adsorption steps since they are not totally decomposed. They form an increasingly thick layer at the surface of the particles of the CuO active phase, which acts as a barrier that limits the diffusion of the incoming gas and thus causes the progressive deactivation of the adsorbent in presence of water vapor. ICP-OES analysis of the regenerated adsorbent indicates that there is still 0.16 wt.% of sulfur (0.11 atomic% of S) after the regeneration at 400 °C at cycle 30 (this low value of 0.16 wt.% is significant since sulfur analysis by ICP-OES performed on the fresh adsorbent which contains no sulfur, indicates a value of sulfur very close to 0: inferior to 0.01 wt.%). The presence of residual sulfur in the adsorbent after the regeneration step, corroborates the formation of such stable sulfur based species. Moreover, the evolution of the $C_{SO_2}^{total}$ data when the H_2O injection is stopped from cycle 31 to 40, also highlights such phenomenon. A progressive recovery of this capacity is then clearly observed, which further confirms the negative impact of water vapor on the performance of the 15CuO/SBA-15 adsorbent at 400 °C. The fact that the increase of $C_{SO_2}^{total}$ is progressive, could mean that the limiting diffusion barrier made by these copper sulfate species can be suppressed at this temperature but at a very slow pace. Therefore, the negative effect of water vapor is reversible at this temperature. This hypothesis is consistent with the evolution of the desorption curves of the 15CuO/SBA-15 adsorbent, observed during the regeneration step at 400 °C (**Figure 3.a**), after the adsorption has been conducted in wet conditions. Indeed, the intensity of the sharp peak observable at the beginning of the

regeneration step (during the first 100 seconds), which corresponds to the fast decomposition of the most accessible copper sulfate species [13], decreases along the first thirty regenerations. This observation indicates that the most accessible sites for SOx trapping (the surface ones) become less and less numerous along the cycles, probably due to the formation of the above-mentioned limiting diffusion barrier, a layer which blocks the copper active sites and which is difficult to regenerate at 400 °C. This behavior is inversed during the regeneration step after adsorption step without water vapor (**Figure 3.b** cycles 31 to 40) and also highlights the reversible character of the deactivation.

When water is injected again (cycles 41 to 50) the regeneration curves have the same shape that the one at cycle 30 (just before stopping H_2O injection) and are similar along cycles indicating a stabilization of the adsorbent (**Figure 3.c**).

At 450 °C, the desorption curves (**Figures 3.d, e, f**) are different from the ones recorded at 400 °C. Indeed, during the 30 first cycles, the sharp peak observable at 400 °C at the beginning of the regeneration step, is not detected at 450 °C. This point underlines a homogeneous decomposition of all the sulfates formed on the CuO active sites at 450 °C. From cycle 31 the desorption curves at 450 °C are different with SO_2 emissions which intensify at the beginning of the regeneration step. This could correspond to the decomposition of different sulfur species (surface and core species), due to the agglomeration of the CuO particles along the cycle sequence.

A schematic representation of the deactivation phenomena is proposed in **Figure 4**. **Figure 4a** illustrates the different competitive reactions at the gas-solid interface during the SO_2 adsorption phase onto the CuO/SBA-15 adsorbent in the presence of H_2O. During the adsorption phases with water vapor, the referent reaction mechanism of SO_2 trapping by SO_2 oxidation to SO_3 and then CuO sulfation as $CuSO_4$ (**Figure 4.a-1**, yellow particles in the scheme) occurs (see equations 1 and 2). In addition, under water vapor, the possible formation of sulfite or sulfate species (**Figure 4.a-2**, blue and yellow particles in the scheme, respectively) offers a second sulfation reaction pathway of the active phase, which could be responsible of the total SO_2 adsorption capacity increase, showing a positive role of water vapor (at 450 °C and at 400 °C on the first cycles). However, the probable competitive adsorption of SO_2, O_2 and H_2O in favor of water vapor on the active sites (**Figure 4.a-3**) could be responsible of the deactivation which is reversible when H_2O injection is stopped. Concerning the formation of non-regenerable sulfated copper species (**Figure 4.a-4,** red particles in the scheme) and their non-decomposition at 400 °C, it leads to the decrease of the SO_2 adsorption capacities, especially the total capacity. The **Figure 4.b** illustrates the active phase evolution along the adsorption/desorption cycles at 400 °C. From cycle 1 to 30, in presence of H_2O, hardly regenerable sulfated Cu-based species are formed during SO_2 adsorption steps (red layer on the scheme) and its thickness increases along the adsorption/regeneration cycles. These species accumulate on the CuO active species which agglomerate along cycles (green particles in the scheme) (**Figure 4.b-1**). As a consequence, $C_{SO_2}^{total}$ decreases. In absence of H_2O, along adsorption/regeneration cycles, (**Figure 4.b-2,** cycle 31 to 40), hardly regenerable sulfated Cu species are no more formed during adsorption steps and are progressively decomposed (decrease of the thickness of the red surface layer) during regeneration steps to form CuO active species (green particles in the scheme) (**Figure 4.b-2**). When H_2O vapor is reintroduced in the gas stream (**Figure 4.b-3,** cycle 41 to 50), a similar behavior to the one of **Figure 4.b-1** is observed**.**

Influence of the CuO active phase loading

When testing the 7CuO/SBA-15 material at 450 °C, no significant evolution of the $C_{SO_2}^{total}$ data is detected when the injection of H_2O vapor is stopped (cycles 31 to 40) (**Figure 1.b**), contrary to what happened with the 15CuO/SBA-15 sample. This is explained by the fact that because of the low amount of copper, the adsorption duration (10,800 s) at 450 °C is sufficient to reach the maximum of its SO_2 adsorption capacity (the sulfation ratio reaching 82 %), regardless of the conditions used during the adsorption step (with and without H_2O). Indeed, this maximum is reached at about 5,000 s with and without water vapor, respectively (**Figures 2.g, h, i**). Consequently, when comparing the performance

of the 7CuO/SBA-15 adsorbent with and without water at 450 °C, no noticeable positive effect of H_2O on the value of $C_{SO_2}^{total}$ is detected.

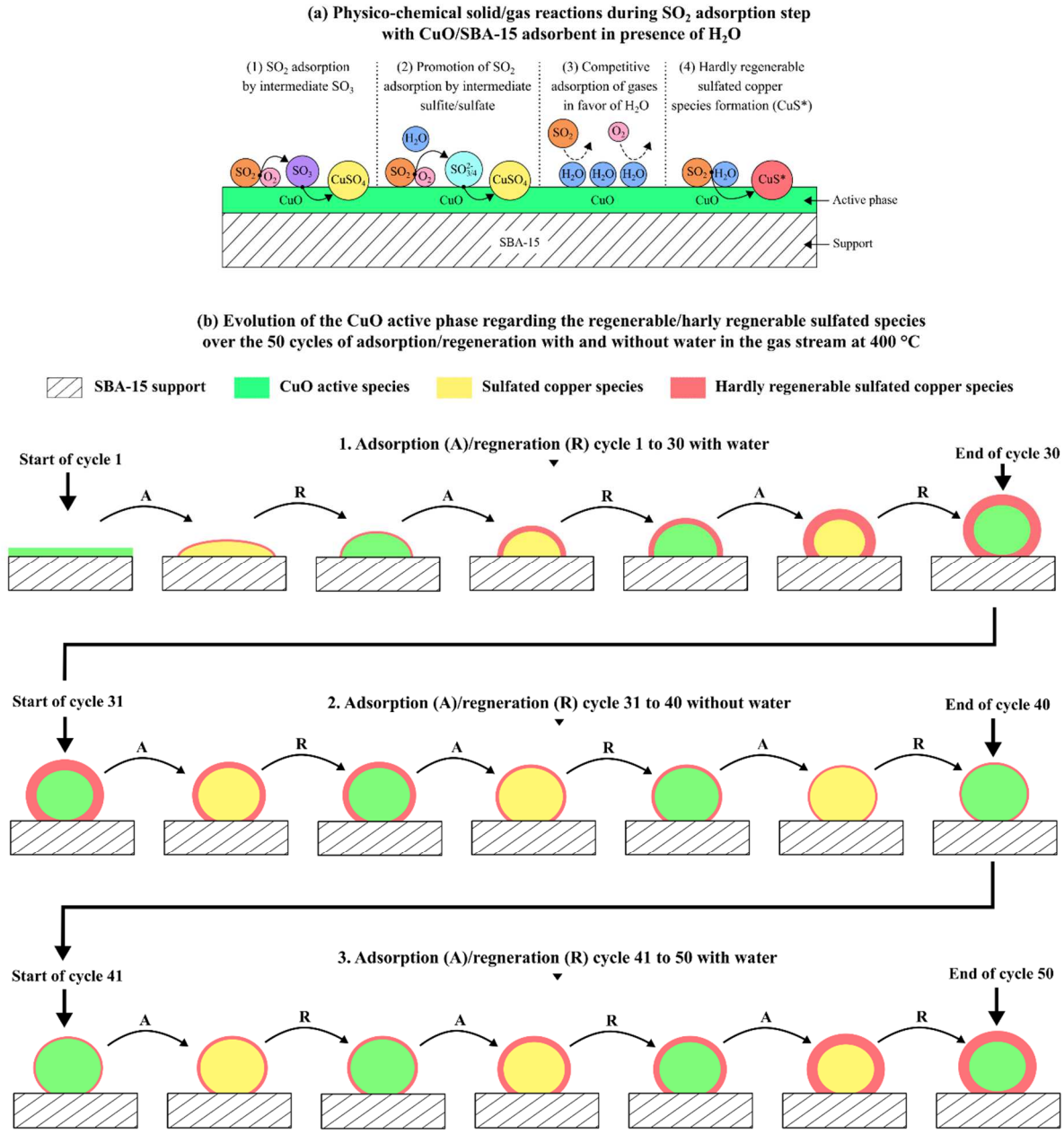

Figure 4: Schematic representation of (a) promotion and deactivation phenomena during the SO_2 adsorption with CuO/SBA-15 in presence of water and (b) evolution of the CuO active phase along the adsorption/desorption cycles at 400 °C regarding the regenerable and hardly regenerable sulfated copper species (For clarity only few cycles are represented).

Influence of the adsorption time

Comparing the evolution *of the* $C_{SO_2}^{breakthrough}$ data of the 15CuO/SBA-15 adsorbent at 450 °C, no sudden change of $C_{SO_2}^{total}$ is noticed when water vapor is removed during experiments where the adsorption steps last 3,000 s (see **Figure 1.b**). While the values of $C_{SO_2}^{breakthrough}$ decrease from cycles 17 to 18 to reach around 100 mg_{SO_2}/g_{CuO} (corresponding to a sulfation ratio of around 12 %) at cycle 50,

the $C_{SO_2}^{total}$ stays constant at around 300 mg_{SO_2}/g_{CuO} (corresponding to a sulfation ratio of around 35 %) over all cycles. The desorption curves are quite similar to each other along cycle sequences (**Figures 3,j, k, l**). They last for about 700 s meaning that sulfated Cu sites represent probably the most accessible fraction of the active sites of the adsorbent. Those less accessible can be sulfated when adsorption time is up to 3,000 s. The $C_{SO_2}^{breakthrough}$ decreases along cycles potentially because of morphological, structural and/or textural changes of the adsorbent along cycles that modify the accessibility to the Cu active sites.

3.2. Structural and textural characterizations of the adsorbents

To understand the structural factors underlying the evolution of the adsorption and regeneration performance of the adsorbents, their structural and textural properties were characterized by XRD, TEM, STEM, EDX and N_2 physisorption manometry after the last cycle of the adsorption/regeneration experiment (the materials being then designated as the "spent" adsorbents), and the characterization results were compared to those of the initial materials (designated as the "fresh" adsorbents).

3.2.1. Transmission Electron Microscopy analyses (TEM, STEM and EDX mapping)

TEM (**Figure 5**) and EDX mapping analyses (**Figure 6**) of the fresh 7CuO/SBA-15 and 15CuO/SBA-15 adsorbents show that the copper active phase is well dispersed in the parallel, ordered (in 2D-hexagonal arrangement) and cylindrical mesopores of the SBA-15 silica support. The interaction between the copper active phase and the support most likely involves species of type Cu^{2+}-O-Si type, which are in strong interaction with the support, as reported in a previous study [12]. As also set out in a previous work [22], transmission electron microscopy analyses performed after all the $DeSO_x$ experiments show that copper-based nanoparticles are present not only in the porosity of the support, with a size similar to the one of the average mesopore diameter (6 nm), but also outside the pores with larger sizes (**Figures 5 and 6**). These particles are formed by the migration and agglomeration of the copper active phase, at a rate depending on the thermal conditions of the $DeSO_x$ experiments:

- Concerning the spent 15CuO/SBA-15 adsorbent, the nanoparticles outside the support pores appear larger and in higher amount at 450 °C than at 400 °C, with a size around 60-90 nm and 50-60 nm, respectively. The increase of temperature from 400 to 450°C actually favors the mobility of the copper active phase particles towards the entrance of the pores of the SBA-15 support, resulting in their migration and coalescence to form larger particles located outside the porosity [22]. This point is also supported by the increase of the variation of dispersion of the CuO active phase after the $DeSO_x$ test at 450 °C (**Figure 6**), which is around 85 % versus 55 % at 400 °C.
- Decreasing the active phase loading (from 15 to 7 wt.%) at 450 °C, the CuO particles of the spent 7CuO/SBA-15 adsorbent that are located outside the pores have sizes around 30-40 nm, a level smaller than the ones found for the spent 15CuO/SBA-15 adsorbent (60-90 nm). Moreover, the variation of the dispersion of the CuO active phase close to 50 %, is lower than the one of the spent 15CuO/SBA-15 adsorbent at 450°C (85 %). This result might reflect that the amount of copper species homogeneously dispersed within the mesopores of the SBA-15 support, is higher at lower concentration.
- Reducing the adsorption duration to 3,000 s at 450°C for a 15CuO/SBA-15 adsorbent, the migration and coalescence of the CuO active phase are reduced. The outside particles have a smaller size of around 20-30 nm (versus around 60-90 nm at 10,800 s) and the variation of dispersion of CuO is lower, equaling 50 % versus around 85 % at 10,800 s. These differences can be assigned to the shorter overall resulting adsorption time after the 50 cycles: 150,000 s (50 x 3,000) vs 540,000 s (50 x 10,800) or 41 h 40’ vs 150 h.

To summarize, the transmission electron microscopy analyses show that the $DeSO_x$ runs induce a process of migration and agglomeration of the CuO active phase resulting in particles located both inside

and outside the support porosity. The growth of the copper-based particles, which depends on the temperature on one hand and on the CuO loading and the adsorption duration on another hand, can partly explain not only the evolution of the breakthrough and total SO_2 adsorption capacities, but also the shape of the adsorption and desorption curves. Adsorption and regeneration phases induced major modifications of the active phase that result in the migration of the Cu active phase to form more or less big particles within and outside the mesoporosity of the support. The extent of the modifications depends mainly on the temperature, the presence of water vapor, the duration of the adsorption phase and on the CuO loadings. These modifications impact directly the accessibility of the active sites since bigger particles (or aggregates) decrease the number of most accessible surface sites in detriment of less accessible core sites. At some point along the cycling process, the shape of the curves, both breakthrough and regeneration, keeps similar, indicating the stabilization of the adsorbent. It is assumed that no more modification of the active phase occurs when stabilization is reached.

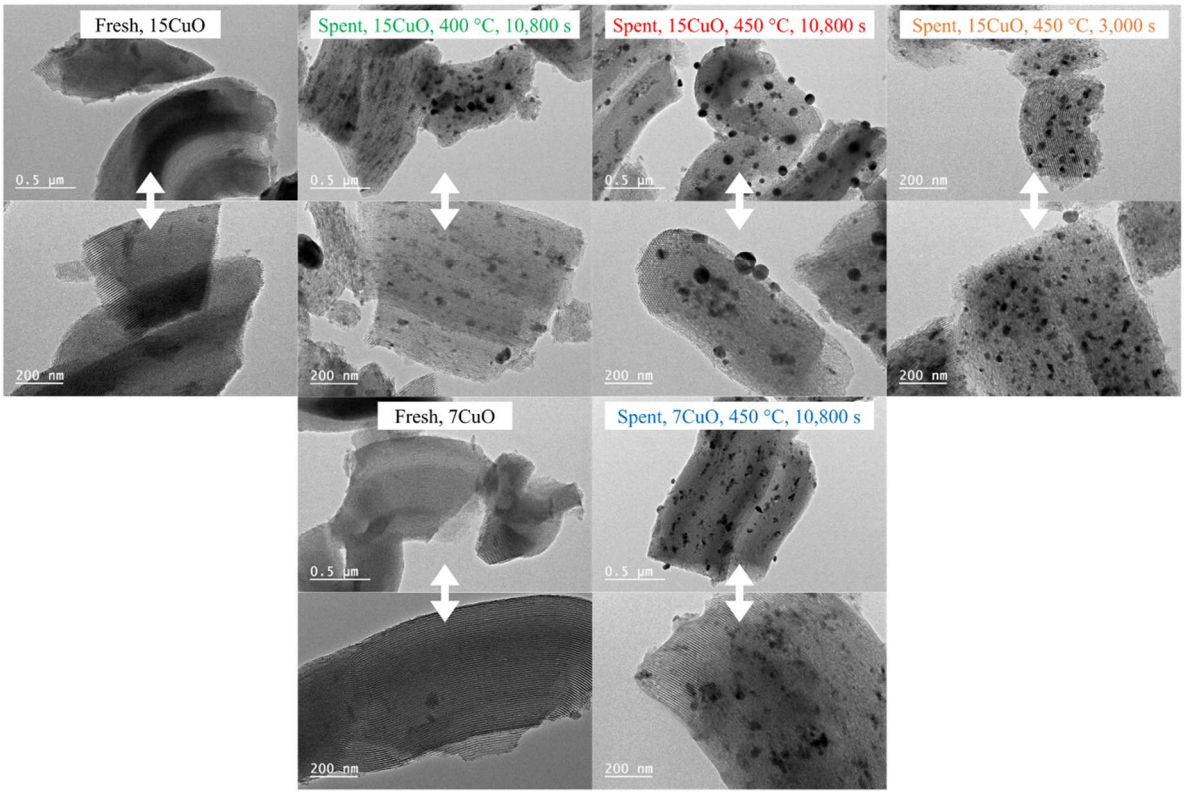

Figure 5: TEM micrographs of the fresh CuO/SBA-15 adsorbents and the spent CuO/SBA-15 adsorbents after 50 SO_2 adsorption/regeneration cycles with or without H_2O during the adsorption step.

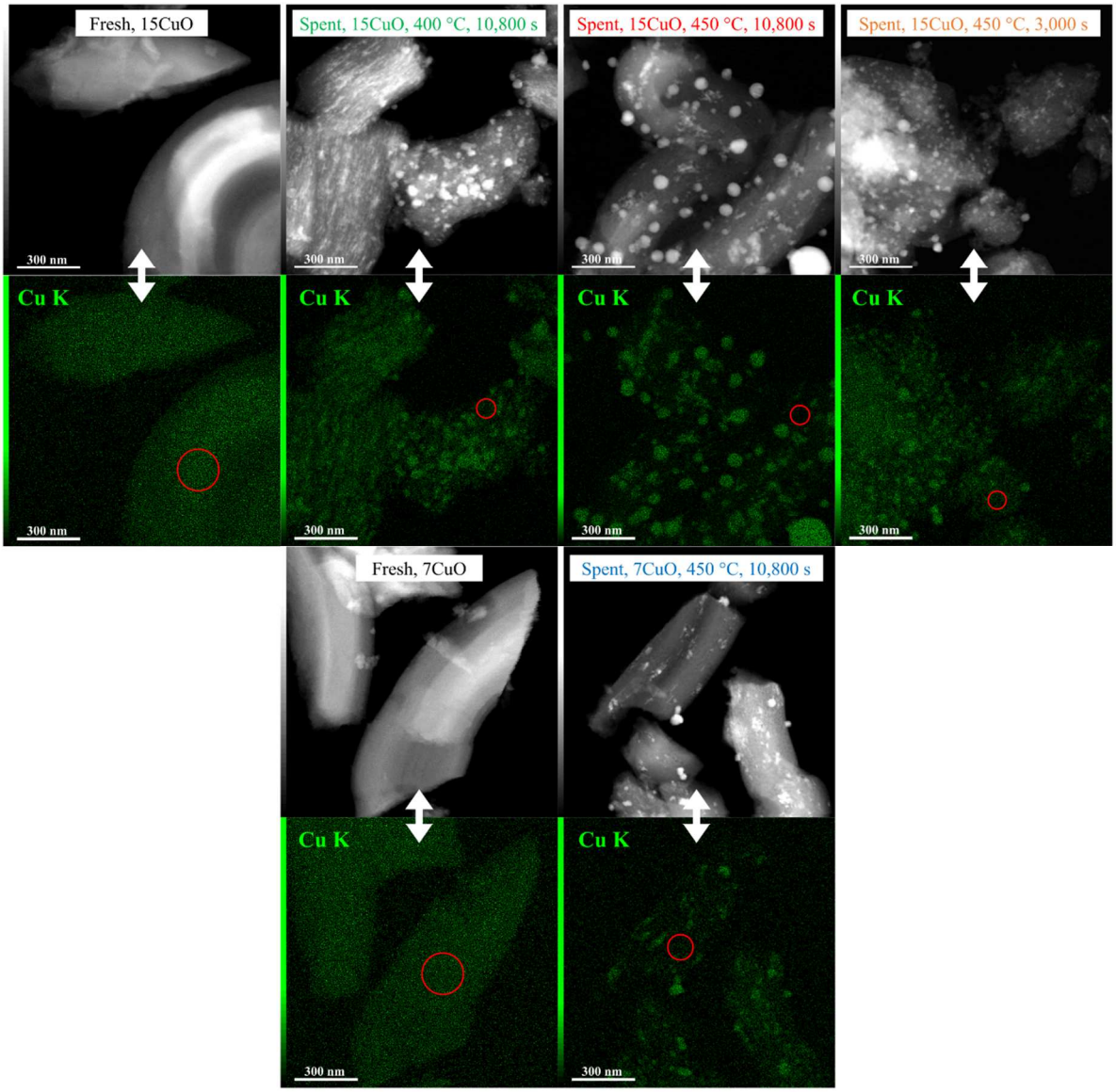

Figure 6: STEM micrographs (Dark field mode) and Cu EDX mappings of the fresh CuO/SBA-15 adsorbents and the spent CuO/SBA-15 adsorbents after 50 SO_2 adsorption/regeneration cycles with or without H_2O during the adsorption step (the red circles represent the selected areas for the CuO dispersion variation).

3.2.2. XRD characterizations

The low and wide-angles XRD patterns of the fresh and spent adsorbents (after cycle 50) are reported in **Figure 7**. Whatever the active phase loading (7 or 15 wt.%), the temperature (400 or 450 °C) and the adsorption duration (3,000 or 10,800 s), the low-angles patterns (**Figure 7a)** show that the organization of the mesoporous network of the adsorbents, which corresponds to the mesoporosity of the SBA-15 support [43], is conserved throughout the cycles. Indeed, the three diffraction peaks, at $2\theta \approx 1.0$, 1.7, and 1.9 °, which correspond to the (100), (110), and (200) reflection planes of the two-dimensional hexagonal packing (*P6mm* space group symmetry) of the cylindrical mesopores, respectively, are observed. However, set out in a previous work [22], we noticed a slight shift of their 2θ position and thus a reduction of the hexagonal lattice parameter from 10.5 to 10 nm on average (see the values in **Table 1**), which is assigned to result from the thermal treatment undergone by the support along the

series of cyclic adsorption /regeneration run [10,44,45]. For the spent adsorbents, the wide-angles XRD patterns (**Figure 7b**) show diffraction peaks corresponding both to the metallic copper (ICDD number: 00-004-0836) and the cuprous oxide (ICDD number: 01-078-2076). These peaks are thinner and more intense at 450 °C with the 15 wt.% CuO loading, compared to the ones observed after cycling at 400 °C and the ones observed after cycling with adsorption duration of 3,000 s at 450 °C with the same 15 wt.% CuO loading. Only one brad and low intense peak characteristics of Cu_2O phase was observed for the spent adsorbent with 7 wt.% CuO loading. These results are in agreement with TEM observations and confirm a greater change in the dispersion of the CuO active phase with the increase of temperature, CuO loading and adsorption duration.

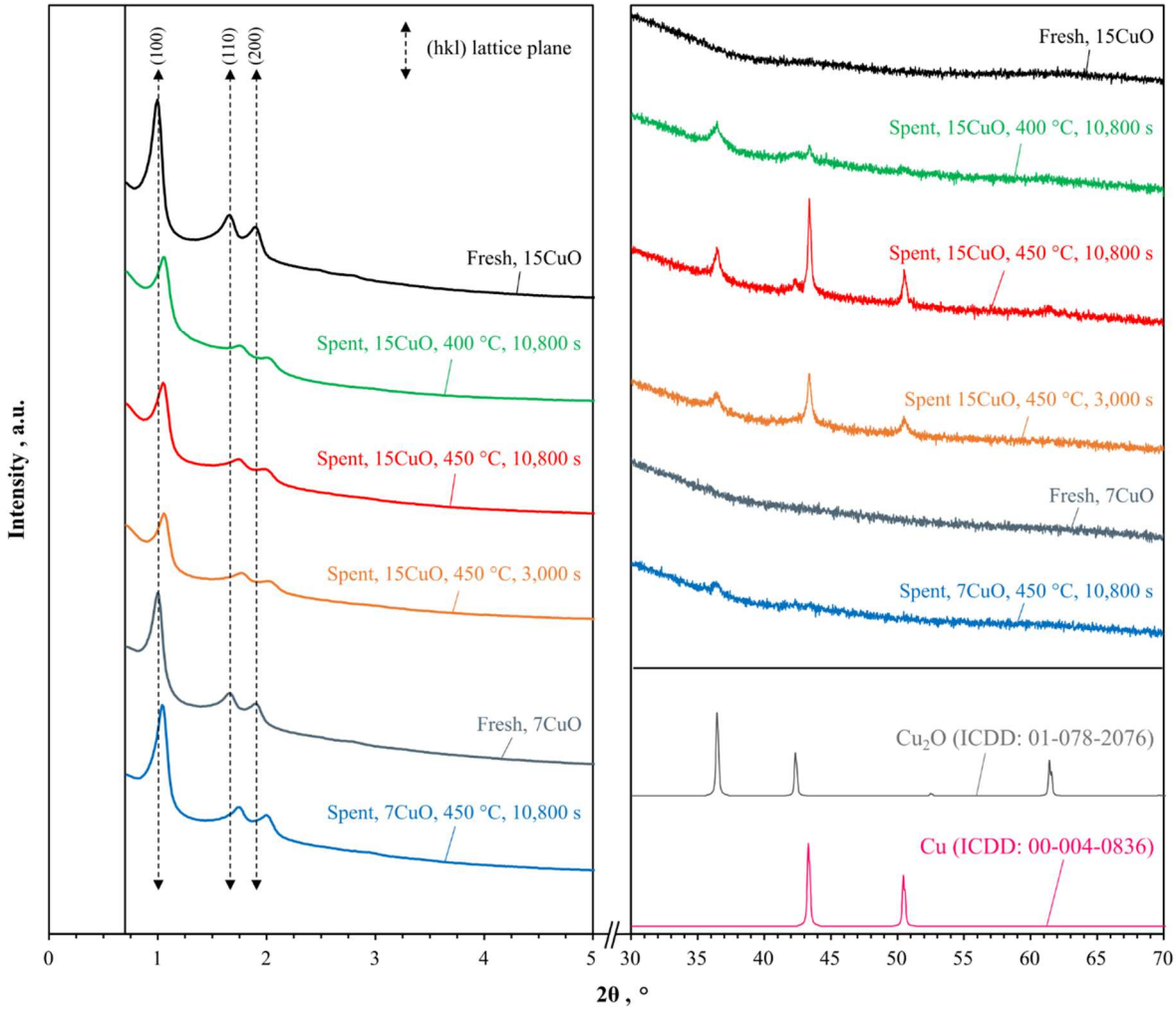

Figure 7: XRD patterns at low (a) and wide (b) 2θ angles ($Cu_{K\alpha}$ radiation) of the fresh CuO/SBA-15 adsorbents and the spent CuO/SBA-15 adsorbents after 50 SO_2 adsorption/regeneration cycles with or without H_2O during the adsorption step.

3.2.3. Nitrogen adsorption/desorption measurements

All the N_2 physisorption isotherms of the fresh and spent CuO/SBA-15 adsorbents (**Figure 8**) exhibit a combination of type I(b) and IV(a) isotherms and a hysteresis of H1 type according to the IUPAC classification [47], this latter hysteresis being characteristic of cylindrical mesopores. For the spent adsorbents at 450 °C, it can be observed that an elongation appears on the adsorption branch towards the high relative pressure at P/P_0 = 0.7-0.9. This feature indicates a deformation of mesopores topology

due to the migration and subsequent particle growth of the CuO active phase inside and outside the porosity, as observed by transmission electron microscopy (**Figures 5 and 6**) and confirmed by the wide angle XRD patterns (**Figure 7b**). In all cases, whatever the temperature of the $DeSO_x$ test and the copper loading, a decrease in the specific surface areas and pore volumes is observed after the SO_2 cycling experiments in dry and wet conditions compared to the ones of the fresh adsorbents (**Table 1**). The micropore volumes are particularly impacted most probably due to the presence of water vapor during the adsorption steps that can promote silanol condensation and partial collapse of micropores.

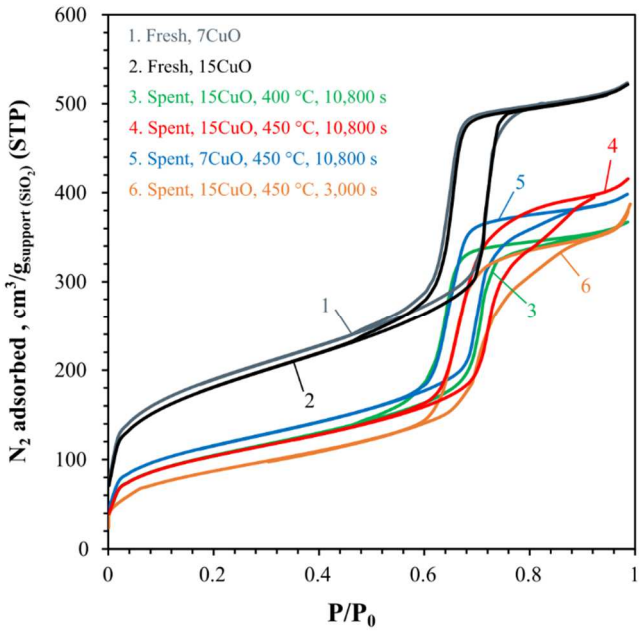

Figure 8: Nitrogen adsorption/desorption isotherms at -196°C of the fresh CuO/SBA-15 adsorbents and the spent CuO/SBA-15 adsorbents after 50 SO_2 adsorption/regeneration cycles with or without H_2O during the adsorption step.

Figure 9 illustrates the modification of the CuO active phase along adsorption/regeneration cycles. The TEM analyses show that the CuO active phase is homogeneously dispersed within the porosity and on the external surface of the fresh CuO/SBA-15 adsorbents (**Figure 9.a**). After the adsorption/regeneration cycles, the CuO active phase has migrate and coalesce to form aggregates inside the mesopores that are observed as nanoparticles whose the size fit the mesopore diameter and larger ones outside the porosity that are observed as big particles located on the surface of the spent CuO/SBA-15 adsorbents (**Figure 9.b**).

The accentuation of the coalescence-migration phenomenon of the active phase (**Figure 9.b**) could disadvantage concurrently the adsorption kinetics of SO_2 and thus generate a decrease of the SO_2 adsorption capacity at the breakthrough as it was observed.

Table 1: Structural and textural properties of the fresh and spent CuO/SBA adsorbents.

Sample	Specific surface area[a] ($m^2/g_{support}$)	Porous volumes[b] ($cm^3/g_{support}$)			Average mesopore diameter[f] (nm)	Hexagonal lattice parameter[g] (nm)	Wall thickness[h] (nm)
		Total[c]	Micro.[d]	Meso.[e]			
Support							
SBA-15	1072	1.14	0.25	0.89	6.5	11	4.5
Fresh adsorbents							
7CuO/SBA-15	683	0.78	0.16	0.63	6.0	10.5	4.5
15CuO/SBA-15	651	0.78	0.15	0.63	6.1	10.5	4.4
Spent adsorbents							
7CuO/SBA-15							
10,800 s							
450 °C	415	0.59	0.09	0.50	5.9	10	4.6
15CuO/SBA-15							
10,800 s							
400 °C	378	0.55	0.08	0.47	5.9	9.9	4.0
450 °C	375	0.60	0.08	0.52	6.3	10	3.7
3,000 s							
450°C	315	0.53	0.07	0.47	6.1	9.9	3.8

[a] *Determined by the BET method [39]*
[b] *Expressed in cm^3 per gram of SiO_2 (silica support alone) and not in cm^3 per gram of adsorbent (active phase + silica support)*
[c] *Total porous volume determined from the N_2 adsorbed volume at $P/P_0 = 0.90$*
[d] *Microporous volume determined from the N_2 adsorbed volume at $P/P_0 = 0.005$ [46]*
[e] *Mesoporous volume calculated from the difference between the total porous volume and the microporous volume*
[f] *Determined by the BJH method on the desorption branch [40]*
[g] *Determined from low 2θ angles XRD pattern*
[h] *Calculated from the difference between the hexagonal lattice parameter and the pore diameter*

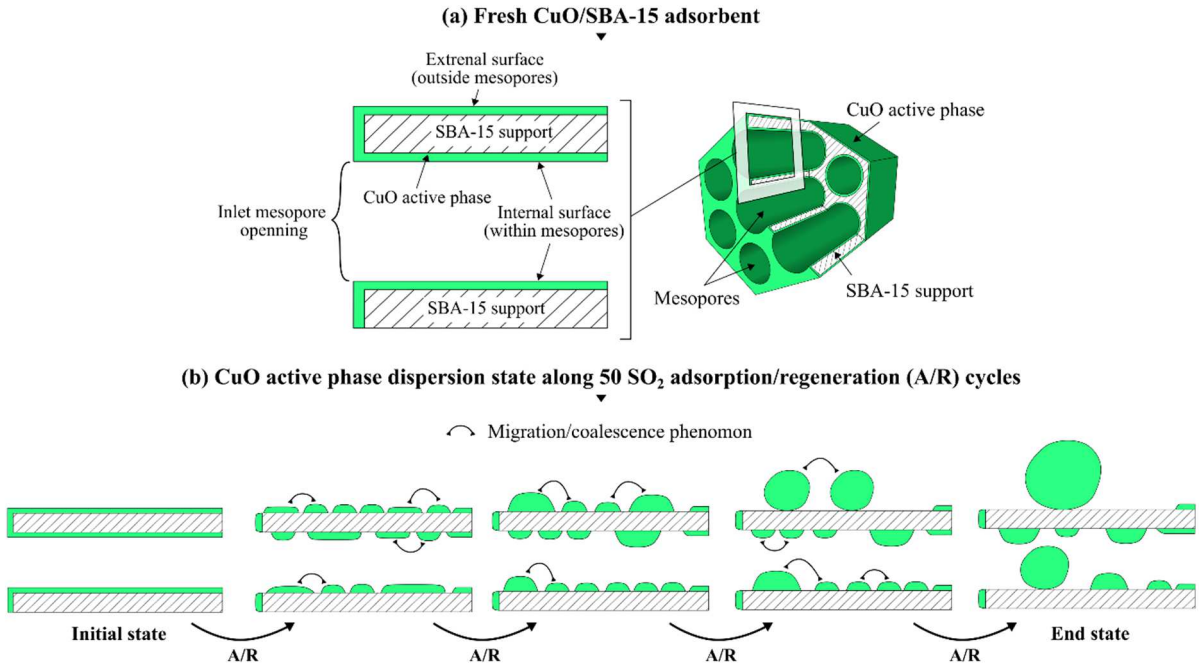

Figure 9: Schematic representation of the dispersion of the CuO active phase for (a) the fresh adsorbents and (b) its evolution along 50 adsorption/regeneration cycles.

4. Conclusion

This work has been motivated by the need to gain a better understanding on the multifaceted role played by H_2O vapor during the adsorption and regeneration of DeSOx materials consisting in CuO supported on SBA-15 mesoporous material. To that end, the approach has been to extensively monitor their adsorption performance - in terms of dynamic and total SO_2 adsorption capacities - throughout several long series of adsorption/regeneration cycles which were alternately conducted in absence and presence of water vapor. This close performance monitoring has been complemented with structural and textural characterizations of the CuO/SBA-15 adsorbent before and after the series of cycles.

The results reveal that the negative impact of water vapor on the SO_2 adsorption capacity of the CuO/SBA-15 adsorbent is partially reversible and dependent of testing parameters as the adsorption temperature, the adsorption time and the copper loading. The changes in the effects of H_2O observed can be explained by the combination of several phenomena, among which the most important seem to be (i) a competitive adsorption of H_2O versus SO_x; (ii) the formation and thermal decomposition of hydroxy-oxy-sulfate species of copper, iii) the mobilization/migration of the copper active phase. An explanatory scheme is proposed and is consistent with the changes observed in the structure and texture of the active copper phase, namely the migration of the copper particles along the pores of the SBA-15 and their coalescence to form large particles, that result partly located outside the pores.

Finally, this study has shown that an increase of the $DeSO_x$ process temperature (from 400 to 450 °C) and a decrease of the copper active phase loading (from 15 to 7 wt.% of CuO) allow to reduce the harmful effects of water vapor on the SO_2 trapping property of the CuO/SBA-15 adsorbent, in particular with respect to the difficult decomposition of some copper sulfate species during a regeneration at 400 °C and the thermal dependence of the migration/coalescence of the active copper phase.

Acknowledgements

The authors would like to thank The French Environment and Energy Management Agency (ADEME), Zéphir Alsace S.A.S and the “Fondation pour l’ENSCMu” for their financial support but also the technical platforms of IS2M for the XRD analyses, nitrogen sorption measurements and electron microscopy analyses.

References

[1] G.E. Likens, T.J. Butler, in: Encyclopedia of the Anthropocene, Elsevier, 2018, pp. 23–31. https://doi.org/10.1016/B978-0-12-809665-9.09977-8.

[2] J.R. Balmes, J.M. Fine, D. Sheppard, Am. Rev. Respir. Dis. 136 (1987) 1117–1121. https://doi.org/10.1164/ajrccm/136.5.1117.

[3] A. De Marco, P. Amoatey, Y.O. Khaniabadi, P. Sicard, P.K. Hopke, Eur. J. Intern. Med. 57 (2018) 49–57. https://doi.org/10.1016/j.ejim.2018.07.027.

[4] R. Zhang, A. Khalizov, L. Wang, M. Hu, W. Xu, Chem. Rev. 112 (2012) 1957–2011. https://doi.org/10.1021/cr2001756.

[5] Le Parlement Européen et le Conseil de l’Union Européenne, Directive (eu) 2016/2284 du parlement européen et du conseil du 14 décembre 2016, 2016.

[6] Economic Commission for Europe, 1999 Protocol to Abate Acidification, Eutrophication and Ground-Level Ozone to the Convention on Longrange Transboundary Air Pollution, as Amended on 4 May 2012, 2013.

[7] T. Lecomte, J.F. Ferrería de la Fuente, F. Neuwahl, M. Canova, A. Pinasseau, I. Jankov, T. Brinkmann, S. Roudier, L. Delgado Sancho, Best Available Techniques (BAT) - Reference Document for Large Combustion Plants: Industrial Emissions Directive 2010/75/EU - Integrated Pollution Prevention and Control, European Commission, 2017.

[8] P. Gaudin, S. Dorge, H. Nouali, M. Vierling, E. Fiani, M. Molière, J.-F. Brilhac, J. Patarin, Appl. Catal. B 181 (2015) 379–388. https://doi.org/10.1016/j.apcatb.2015.08.011.

[9] P. Gaudin, S. Dorge, H. Nouali, J. Patarin, J.-F. Brilhac, E. Fiani, M. Vierling, M. Molière, C. R. Chim. 18 (2015) 1013–1029. https://doi.org/10.1016/j.crci.2015.07.002.

[10] P. Gaudin, L. Michelin, L. Josien, H. Nouali, S. Dorge, J.-F. Brilhac, E. Fiani, M. Vierling, M. Molière, J. Patarin, Fuel Process. Technol. 148 (2016) 1–11. https://doi.org/10.1016/j.fuproc.2016.02.025.

[11] P. Gaudin, P. Fioux, S. Dorge, H. Nouali, M. Vierling, E. Fiani, M. Molière, J.-F. Brilhac, J. Patarin, Fuel Process. Technol. 153 (2016) 129–136. https://doi.org/10.1016/j.fuproc.2016.07.015.

[12] M. Berger, P. Fioux, S. Dorge, H. Nouali, D. Habermacher, E. Fiani, M. Vierling, J. Patarin, J.-F. Brilhac, Catal. Sci. Technol. 7 (2017) 4115–4128. https://doi.org/10.1039/C7CY01010A.

[13] M. Berger, H. Nouali, S. Dorge, D. Habermacher, E. Fiani, M. Vierling, M. Molière, C. Schönnenbeck, J.-F. Brilhac, J. Patarin, Chem. Eng. J. 347 (2018) 202–213. https://doi.org/10.1016/j.cej.2018.04.066.

[14] M. Berger, S. Dorge, H. Nouali, D. Habermacher, E. Fiani, M. Vierling, M. Molière, J.F. Brilhac, J. Patarin, Chem. Eng. J. 350 (2018) 729–738. https://doi.org/10.1016/j.cej.2018.05.170.

[15] M. Berger, S. Dorge, H. Nouali, D. Habermacher, E. Fiani, M. Vierling, M. Molière, J.F. Brilhac, J. Patarin, Chem. Eng. J. 384 (2020) 123318. https://doi.org/10.1016/j.cej.2019.123318.

[16] M. Berger, A. Brillard, S. Dorge, D. Habermacher, H. Nouali, P. Kerdoncuff, M. Vierling, M. Molière, J. Patarin, J.-F. Brilhac, J. Hazard. Mater. 385 (2020) 121579. https://doi.org/10.1016/j.jhazmat.2019.121579.

[17] P. Shah, V. Ramaswamy, Micropor. Mesopor. Mat. 114 (2008) 270–280. https://doi.org/10.1016/j.micromeso.2008.01.013.

[18] X. Zhang, G. Zhuang, J. Chen, Y. Wang, X. Wang, Z. An, P. Zhang, J. Phys. Chem. B 110 (2006) 12588–12596. https://doi.org/10.1021/jp0617773.

[19] W.G. Davenport, M.J. King, B. Rogers, A. Weissenberger, in: R.T. Jones, Johannesburg, 2006, p. 16.

[20] W.G. Davenport, M.J. King, in: W.G. Davenport, M.J. King (Eds.), Sulfuric Acid Manufacture, Elsevier, Oxford, 2006, pp. 11–17. https://doi.org/10.1016/B978-008044428-4/50002-6.

[21] S.G. Nelson, Coal Sci. Technol. 21 (1993) 543–554. https://doi.org/10.1016/B978-0-444-81476-0.50047-8.

[22] G. Guicheney, S. Dorge, H. Nouali, B. Lebeau, M. Soulard, J. Patarin, M. Molière, M. Vierling, A.C. Houdon, J.F. Brilhac, Catal. Today (2021). https://doi.org/10.1016/j.cattod.2021.07.018.

[23] Z. Chen, H. Ge, P. Wang, J. Sun, M. Abbas, J. Chen, Mol. Catal. 488 (2020) 110919. https://doi.org/10.1016/j.mcat.2020.110919.

[24] J.W. Park, J.H. Jeong, W.L. Yoon, Y.W. Rhee, J. Power Sources 132 (2004) 18–28. https://doi.org/10.1016/j.jpowsour.2003.12.059.

[25] F. Gao, X. Tang, H. Yi, S. Zhao, C. Li, J. Li, Y. Shi, X. Meng, Catalysts 7 (2017) 199. https://doi.org/10.3390/catal7070199.

[26] G. Qi, R.T. Yang, R. Chang, Appl. Catal. B 51 (2004) 93–106. https://doi.org/10.1016/j.apcatb.2004.01.023.

[27] D. Qiao, G. Lu, Y. Guo, Y. Wang, Y. Guo, J. Rare Earths 28 (2010) 742–746. https://doi.org/10.1016/S1002-0721(09)60192-7.

[28] M. Iwamoto, N. Mizuno, H. Yahiro, Stud. Surf. Sci. Catal. 75 (1993) 1285–1298. https://doi.org/10.1016/S0167-2991(08)64451-1.

[29] W.S. Kijlstra, J.C.M.L. Daamen, J.M. Van de Graaf, B. Der Linden, E.K. Poels, A. Bliek, Appl. Catal. B 7 (1996) 337–357. https://doi.org/10.1016/0926-3373(95)00052-6.

[30] G. Liu, W. Zhang, P. He, S. Guan, B. Yuan, R. Li, Y. Sun, D. Shen, Catalysts 9 (2019) 289. https://doi.org/10.3390/catal9030289.

[31] R. Gholami, M. Alyani, K. Smith, Catalysts 5 (2015) 561–594. https://doi.org/10.3390/catal5020561.

[32] Z. Wu, H. Zhu, Z. Qin, H. Wang, J. Ding, L. Huang, J. Wang, Fuel 104 (2010) 41–45. https://doi.org/10.1016/j.fuel.2010.03.001.

[33] Y. Osaka, K. Iwai, T. Tsujiguchi, A. Kodama, H. Huang, Environ. Technol. (2019) 1–7. https://doi.org/10.1080/09593330.2019.1614095.

[34] C. Laguerie, D. Barreteau, Sadhana 10 (1987) 49–67. https://doi.org/10.1007/BF02816197.

[35] R. Lamber, N. Jaeger, G. Schulz-Ekloff, J. Catal. 123 (1990) 285–297. https://doi.org/10.1016/0021-9517(90)90128-7.

[36] Q. Xu, K.C. Kharas, B.J. Croley, A.K. Datye, ChemCatChem 3 (2011) 1004–1014. https://doi.org/10.1002/cctc.201000392.

[37] H. Tong, J. Dai, Y. He, Z. Tong, Environ. Technol. 32 (2011) 891–900. https://doi.org/10.1080/09593330.2010.517219.

[38] A. Galarneau, F. Villemot, J. Rodriguez, F. Fajula, B. Coasne, Langmuir 30 (2014) 13266–13274. https://doi.org/10.1021/la5026679.

[39] S. Brunauer, P.H. Emmett, E. Teller, J. Am. Chem. Soc. 60 (1938) 309–319. https://doi.org/10.1021/ja01269a023.

[40] E.P. Barrett, L.G. Joyner, P.P. Halenda, J. Am. Chem. Soc. 73 (1951) 373–380. https://doi.org/10.1021/ja01145a126.

[41] I. Uzunov, D. Klissurski, L. Teocharov, J. Therm. Anal. Calorim. 44 (1995) 685–696. https://doi.org/10.1007/BF02636286.

[42] G. Lachenal, J.R. Vignalou, Thermochimic. Acta 64 (1983) 207–227. https://doi.org/10.1016/0040-6031(83)80144-0.

[43] D. Zhao, J. Feng, Q. Huo, N. Melosh, G.H. Fredrickson, B.F. Chmelka, G.D. Stucky, Science 279 (1998) 548–552. https://doi.org/10.1126/science.279.5350.548.

[44] T. Benamor, L. Michelin, B. Lebeau, C. Marichal, Micropor. Mesopor. Mat. 147 (2012) 334–342. https://doi.org/10.1016/j.micromeso.2011.07.004.

[45] F. Bérubé, S. Kaliaguine, Micropor. Mesopor. Mat. 115 (2008) 469–479. https://doi.org/10.1016/j.micromeso.2008.02.028.

[46] A. Galarneau, F. Villemot, J. Rodriguez, F. Fajula, B. Coasne, Langmuir 30 (2014) 13266–13274. https://doi.org/10.1021/la5026679.

[47] M. Thommes, K. Kaneko, A.V. Neimark, J.P. Olivier, F. Rodriguez-Reinoso, J. Rouquerol, K.S.W. Sing, Pure Appl. Chem. 87 (2015) 1051–1069. https://doi.org/10.1515/pac-2014-1117.